

Appendix B

Tidal

Appendix B. Tidal

B1. HRCS Model Configuration

The model (HRCS) has been set up over the domain of the NW European continental shelf shown in Figure B1.1. Horizontal grid resolution is $1/60^\circ$ latitude by $1/40^\circ$ longitude (approximately 1.8 km) and there are 34 levels in the vertical.

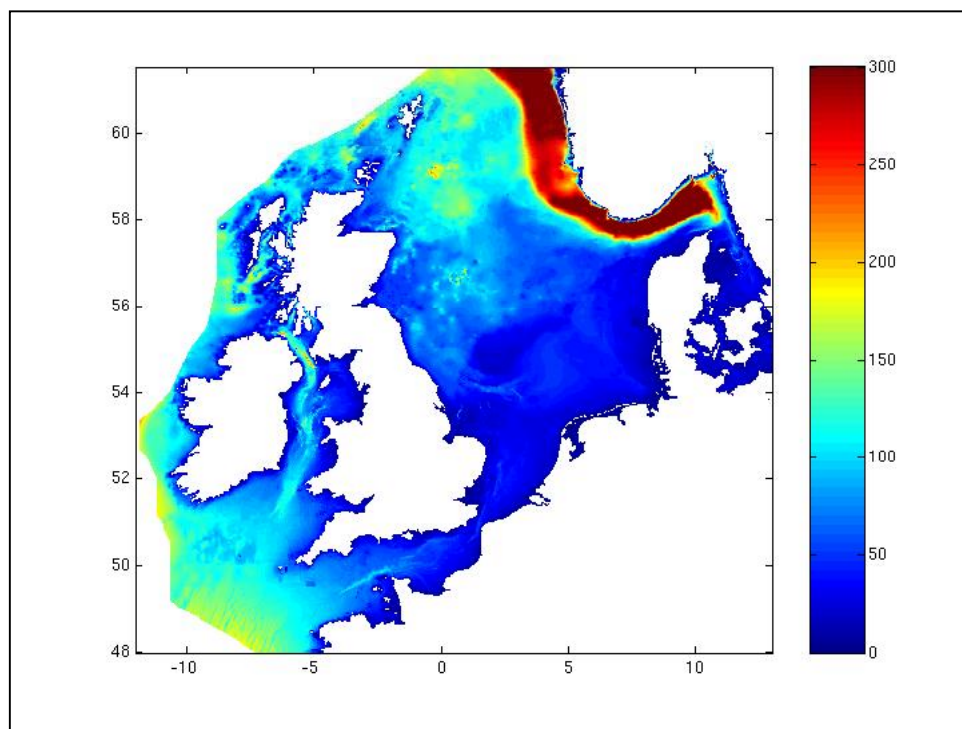


Figure B1.1 Domain of HRCS (High Resolution Continental Shelf) model and depths (m)

Bathymetry for this model domain has been constructed from a variety of sources. The underlying bathymetry originates from the GEBCO (General Bathymetric Chart of the Oceans) 1 minute digitised bathymetry. This data has been interpolated onto the $1/40^\circ$ longitude by $1/60^\circ$ latitude grid of HRCS and the model coastline guided (but not defined) by the World Vector Shoreline. Where possible, the bathymetry has been improved by the replacement of the GEBCO depths with bathymetry from higher resolution datasets available to POL. This has provided significant improvements over GEBCO bathymetry in near-shore inter-tidal regions.

The model, an adaptation of Proctor & James (1996), solves the 3-dimensional incompressible, Boussinesq, hydrostatic equations in spherical polar coordinates with a transformed vertical coordinate, σ . The equations used are:

$$\begin{aligned} \frac{\partial u}{\partial t} = & -L(u) + \left(f + \frac{u \tan \varphi}{R} \right) v - \frac{1}{R \cos \varphi} \left(\frac{\partial \Phi}{\partial \chi} - \left[\frac{\partial \zeta}{\partial \chi} + \sigma \frac{\partial D}{\partial \chi} \right] b \right) \\ & - \frac{1}{\rho_o R \cos \varphi} \frac{\partial P_a}{\partial \chi} + \frac{1}{D^2} \frac{\partial}{\partial \sigma} \left(A \frac{\partial u}{\partial \sigma} \right) \end{aligned} \quad (1)$$

$$\begin{aligned} \frac{\partial v}{\partial t} = & -L(v) - \left(f + \frac{u \tan \varphi}{R} \right) u - \frac{1}{R} \left(\frac{\partial \Phi}{\partial \varphi} - \left[\frac{\partial \zeta}{\partial \varphi} + \sigma \frac{\partial D}{\partial \varphi} \right] b \right) \\ & - \frac{1}{\rho_o R} \frac{\partial P_a}{\partial \varphi} + \frac{1}{D^2} \frac{\partial}{\partial \sigma} \left(A \frac{\partial v}{\partial \sigma} \right) \end{aligned} \quad (2)$$

$$\frac{\partial b}{\partial t} = -L(b) + \frac{1}{D^2} \frac{\partial}{\partial \sigma} \left(K \frac{\partial b}{\partial \sigma} \right) \quad (3)$$

where :

- u, v and Ω = the positive velocity components in east (χ), north (φ) and vertical (σ) directions respectively;
- D = total depth ($= H + \zeta$);
- ζ = surface elevation above mean sea level;
- f = the Coriolis parameter;
- P_a = the atmospheric pressure;
- Φ = (total pressure $P - P_a$)/ $\rho_o + gz$;
- b = buoyancy = $g (\rho_o - \rho) / \rho_o$;
- A = the coefficient of vertical viscosity; and
- K = the coefficient of vertical diffusivity.

The non-linear terms, $L(a)$, are given by:

$$L(a) = \frac{u}{R \cos \varphi} \frac{\partial a}{\partial \chi} + \frac{v}{R} \frac{\partial a}{\partial \varphi} + \Omega \frac{\partial a}{\partial \sigma} \quad (4)$$

where:

Ω is the velocity component in the vertical (σ) direction given by:

$$\Omega = -\frac{\sigma}{D} \frac{\partial \zeta}{\partial t} - \frac{1}{DR \cos \varphi} \left[\frac{\partial}{\partial \chi} \left(D \int_0^\sigma u d\sigma \right) + \frac{\partial}{\partial \varphi} \left(D \cos \varphi \int_0^\sigma v d\sigma \right) \right] \quad (5)$$

also:

$$b = \frac{1}{D} \frac{\partial \Phi}{\partial \sigma} \quad (6)$$

so

$$\Phi = D \int_0^\sigma b d\sigma + g\zeta. \quad (7)$$

The vertical coordinate is $\sigma = (z - \zeta) / (H + \zeta)$, and the interior water column is divided into N-2 (where N=34) σ levels. To maintain resolution near the surface in deep water the σ spacing is allowed to vary in the horizontal according to the transformation

$$\begin{aligned} \sigma_{k-0.5} &= S_k + \frac{h_{i,j} - h_c}{h_{i,j}} [C(S_k) - S_k] & h_{i,j} > h_c \\ &= S_k & h_{i,j} \leq h_c \end{aligned} \quad (8)$$

where:

S_k are N-1 evenly spaced levels between $\sigma = -1$ and $\sigma = 0$ and $C(S_k)$ is defined as

$$C(S_k) = (1 - B) \frac{\sinh(\theta S_k)}{\sinh \theta} + B \frac{\tanh(\theta[S_k + 0.5]) - \tanh(0.5\theta)}{2 \tanh(0.5\theta)}. \quad (9)$$

This follows from the s coordinate transformation of Song & Haidvogel (1994) except we retain the definition of σ i.e. the levels in σ space do not vary with time. Parameters h_c , θ and B can be tuned to give increased resolution at the surface and / or at the sea bed. In depths shallower than h_c the standard σ levels are used, for depths greater than h_c the transformation is invoked. It should be noted that in this application, where water depths on the continental shelf are mostly less than 150m, only the σ coordinate is used.

For numerical efficiency the equations are split into their depth-mean components and 3-dimensional deviations, the depth-mean equations are:

$$\frac{\partial \bar{u}}{\partial t} = f\bar{v} - \frac{g}{R \cos \varphi} \frac{\partial \zeta}{\partial \chi} - \frac{1}{\rho_0 R \cos \varphi} \frac{\partial P_a}{\partial \chi} - \frac{1}{D} F_B + NLB_\chi \quad (10)$$

$$\frac{\partial \bar{v}}{\partial t} = -f\bar{u} - \frac{g}{R} \frac{\partial \zeta}{\partial \varphi} - \frac{1}{\rho_0 R} \frac{\partial P_a}{\partial \varphi} - \frac{1}{D} G_B + NLB_\varphi \quad (11)$$

where :

F_B, G_B = components of bottom stress given by

$$(F_B, G_B) = C_{DB} (u_b, v_b) \sqrt{(u_b^2 + v_b^2)}. \quad (12)$$

where :

u_b, v_b = components of bottom current;

C_{DB} = bottom stress coefficient (set to $\left[\kappa^{-1} \log\left(\frac{\delta}{z_0}\right) \right]^{-2}$, $C_{DB} > 0.005$,

where:

δ is depth of u_b, v_b above the seabed, $z_0 = 0.003$ and κ is von Karman's constant (= 0.41); and

NLB_χ and NLB_ϕ are depth-means of the non-linear and buoyancy terms held constant through the depth mean solution:

$$NLB_\chi = \int_{-1}^0 \left[-L(u) + \frac{uv \tan \phi}{R} - \frac{1}{R \cos \phi} \left(\frac{\partial}{\partial \chi} \left[D \int_0^\sigma b d\sigma \right] - \left[\frac{\partial \zeta}{\partial \chi} + \sigma \frac{\partial D}{\partial \chi} \right] b \right) \right] d\sigma \quad (13)$$

$$NLB_\phi = \int_{-1}^0 \left[-L(v) + \frac{u^2 \tan \phi}{R} - \frac{1}{R} \left(\frac{\partial}{\partial \phi} \left[D \int_0^\sigma b d\sigma \right] - \left[\frac{\partial \zeta}{\partial \phi} + \sigma \frac{\partial D}{\partial \phi} \right] b \right) \right] d\sigma \quad (14)$$

The continuity equation is:

$$\frac{\partial \zeta}{\partial t} + \frac{1}{R \cos \phi} \left[\frac{\partial}{\partial \chi} (D \bar{u}) + \frac{\partial}{\partial \phi} (D \cos \phi \bar{v}) \right] = 0 \quad (15)$$

For velocity deviations from the depth mean, $u_r = u - \bar{u}$, $v_r = v - \bar{v}$:

$$\begin{aligned} \frac{\partial u_r}{\partial t} = & -L(u) + f v_r + \frac{uv \tan \phi}{R} - \frac{1}{R \cos \phi} \left(\frac{\partial}{\partial \chi} \left[D \int_0^\sigma b d\sigma \right] \right. \\ & \left. - \left[\frac{\partial \zeta}{\partial \chi} + \sigma \frac{\partial D}{\partial \chi} \right] b \right) + \frac{1}{D^2} \frac{\partial}{\partial \sigma} \left(A \frac{\partial u}{\partial \sigma} \right) + \frac{1}{D} F_B - NLB_\chi \end{aligned} \quad (16)$$

$$\begin{aligned} \frac{\partial v_r}{\partial t} = & -L(v) - f u_r - \frac{u^2 \tan \phi}{R} - \frac{1}{R} \left(\frac{\partial}{\partial \phi} \left[D \int_0^\sigma b d\sigma \right] \right. \\ & \left. - \left[\frac{\partial \zeta}{\partial \phi} + \sigma \frac{\partial D}{\partial \phi} \right] b \right) + \frac{1}{D^2} \frac{\partial}{\partial \sigma} \left(A \frac{\partial v}{\partial \sigma} \right) + \frac{1}{D} G_B - NLB_\phi \end{aligned} \quad (17)$$

The equation for salinity S is:

$$\frac{\partial S}{\partial t} = -L(S) + \frac{1}{D^2} \frac{\partial}{\partial \sigma} \left(K \frac{\partial S}{\partial \sigma} \right) \quad (18)$$

and a similar equation for temperature T :

$$\frac{\partial T}{\partial t} = -L(T) + \frac{1}{D^2} \frac{\partial}{\partial \sigma} \left(K \frac{\partial T}{\partial \sigma} \right) \quad (19)$$

S and T are linked to give buoyancy b by an equation of state $b = b(T, S)$ (Gill 1982).

It should be noted that in these tide-only simulations, buoyancy terms are omitted, S and T are held constant and there is no advection of S or T . The water column is assumed to be temporally and spatially homogeneous.

A turbulence closure scheme is used, based on the Mellor-Yamada "level 2.5" turbulent energy model (Mellor & Yamada, 1974), with algebraic mixing lengths as described by Galperin *et al.* (1988). This scheme includes turbulent kinetic energy as a prognostic variable. The scheme gives better results than the previously used Richardson number scheme, particularly in the depth and sharpness of the seasonal thermocline. The flux of turbulence from surface wave breaking is included through the Craig & Banner (1994) formulation. A small value of background viscosity is chosen to be $10^{-5} \text{ m}^2\text{s}^{-1}$ to allow for diapycnal mixing. Horizontal viscosity and diffusion is included, based on the Smagorinsky shear-dependent formulation described by Oey (1998).

An important component of the numerical solution is the advection scheme. In shallow seas with strong tidal advection, numerical diffusion can be excessive and erode the density structure (James 1986). For long time integrations such as those envisaged with this model (>1 year) a feature-preserving scheme is vital to the model's success. We adopt the PPM (piecewise parabolic method) scheme (Colella & Woodward 1984). This method ensures conservation and positivity, has excellent feature preserving properties (James 1996) and is not limited by a vertical CFL condition (James 2000).

On the open sea boundaries the model uses a "radiation" condition to prescribe the forcing. This takes the form:

$$q - (q_T + q_M + q_D) = (c / H)(\zeta - (\zeta_T + \zeta_M + \zeta_D)) \quad (20)$$

where :

$$c = \sqrt{gH}$$

This allows depth-averaged tidal current and surface elevation (q_T, ζ_T), meteorological driven motion (q_M, ζ_M) and density driven motion (q_D, ζ_D) to be input, whilst allowing internally generated gravity waves to propagate out of the model domain. Such a radiation scheme has been used highly successfully in tide and storm surge models (Flather et al. 1991). On closed boundaries there is no normal flow. It should be noted that meteorological terms (M) and density driven terms (D) are not included in these simulations. Tidal forcing is derived from a set of tidal constituents (15) specified around the open boundaries of the domain (shown in Figure B1.1) from the NS3 model, i.e.

$$\zeta_T(s, t) = \sum_i f_i H_i(s) \cos(\omega_i t - G_i(s) + U_i + V_i) \quad (21)$$

where :

- t = time,
- H_i = amplitude of the tidal elevation constituent i at position $s(\chi, \varphi)$ on the open boundary
- G_i = phase of the tidal elevation constituent i at position $s(\chi, \varphi)$ on the open boundary,
- ω_i = the phase speed of tidal constituent i ;
- V_i = phase at time t_0 relative the Greenwich, and
- f_i & U_i = nodal corrections for the 18.6 year nodal variation.

The depth-averaged q_T is given in a similar manner. Values of H and G for both ζ_T and q_T are obtained from a larger area Atlantic Margin Model (AMM). The AMM is run operationally at the Met Office and :

- covers the north-west European continental shelf and much of the shelf break to the west of the British Isles;
- has a resolution of $1/9^\circ$ latitude and $1/6^\circ$ longitude;
- is fully baroclinic with prognostic temperature and salinity, representing dynamical processes both on the shelf and in deeper water;
- has a state-of-the-art piecewise parabolic advection scheme to preserve strong gradients and minimise diffusion, even with advection over many tidal cycles;
- is driven by hourly winds and pressures, and three-hourly heat fluxes from the Met Office mesoscale model;
- uses sigma (terrain-following) vertical co-ordinates with 14 model levels;
- includes tidal forcing (15 harmonic constituents) at Atlantic boundaries; and
- takes freshwater inputs from 47 sources (rivers and the Baltic).

The data from the AMM are interpolated on to the HRCS open boundary points. Tide generating forces (the 'equilibrium tide') are not directly included in HRCS simulations because the waters on the shelf are only affected by these forces to a second order. The forces are included, however, in the AMM which produces the open boundary forcing for HRCS.

At the sea surface heat and salt (precipitation-evaporation) fluxes may be prescribed via bulk formulae or obtained directly from an atmospheric model but, in these barotropic simulations, are not input. At the sea bed there is zero heat and salt flux. Likewise, rivers may be represented as a freshwater inflow having a given volume flux at a given salinity extending over a given depth but these are not included in the tidal simulations.

The equations are solved in finite difference form on an Arakawa B grid. James (1986) has shown that the B grid (Figure B1.2) has superior properties for the preservation of sharp fronts, because there is less numerical diffusion introduced at the velocity points than with the more usually adopted C grid. An explicit, forward-time, centred-space scheme is used to solve the momentum and scalar equations, with an implicit (Crank-Nicholson) solver for vertical diffusion. A full description of the hydrodynamic model can be found in Holt & James (2001).

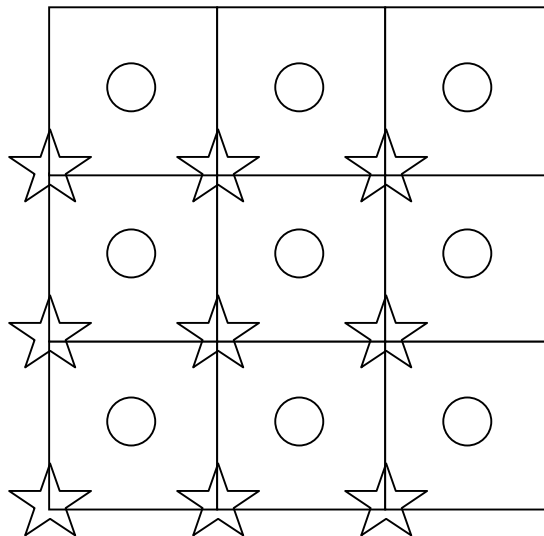


Figure B1.2 B-grid schematisation: locations of depth and surface elevation points (o), east (u) & north (v) velocity points (star)

The model code has been parallelised (using Message Passing Interface (MPI-1) processes) to run efficiently on a range of machines such as the Cray T3E, SG Origin 3800, the SGI Altix 3700, the IBM pSeries 690 *Regatta* (HPCx), and the POL 128 processor Linux PC cluster (where the model runs were carried out). The hydrodynamics provide the framework for POLCOMS (the Proudman Oceanographic Laboratory Coastal Ocean Modelling System, www.pol.ac.uk/home/research/polcoms), a multi-disciplinary modelling system including hydrodynamics, sediment dynamics, ecosystem dynamics and lagrangian particle tracking. Aspects of the system's performance can be found in Ashworth *et al.* (2002) and studies of physics, ecosystem and sediment dynamics are described in {Holt *et al.*, (2001), Holt and Proctor (2003)}, {Allen *et al.* (2001), Holt *et al.* (2004)} and Proctor *et al.* (2001) respectively.

References

- Allen, J.I., Blackford, J., Holt, J.T., Ashworth, M.I. Proctor, R., & Siddorn, J. 2001: A highly spatially resolved ecosystem model for the northwest European continental shelf. *Sarsia*, 86: 423-440.
- Ashworth, M., Proctor, R., Holt, J.T., Allen, J.I. & Blackford, J.C. 2002: Coupled marine ecosystem modelling on high performance computers. In *Developments in Teracomputing*, eds. W. Zwiefelhofer and N. Kreitz, 2001, pp. 150-163, (World Scientific).
- Colella, P., Woodward, P. R. 1984: The piecewise parabolic method (PPM) for gas-dynamical simulations. *Journal of Computational Physics* 54: 174-201.
- Craig, P.D. & Banner, M.L. 1994: Modelling wave-enhanced turbulence in the ocean surface layer. *J. Phys. Oceanog.*, 24: 2546-2559.
- Flather, R. A., Proctor, R., Wolf, J. 1991: Oceanographic forecast models. In: Farmer, D. G., Rycroft, M. J. eds. *Computer modelling in the environmental sciences*. pp. 15-30 Clarendon Press, Oxford.
- Galperin B., Kantha L. H., Hassid S. and Rossati A. 1988: A quasi-equilibrium turbulent energy model for geophysical flows. *Journal of Atmospheric Sciences* 45: 55-62
- Gill, A. E. 1982: *Atmosphere-Ocean Dynamics*. International Geophysics Series 30. Academic Press, New York. 662 p.
- Holt, J.T. and James, I.D. 2001: An S coordinate density evolving model of the northwest European shelf: 1, Model description and density structure. *J. Geophys. Res.*, 106, C7: 14015-14034.
- Holt, J.T., Proctor, R., 2003. The role of advection in determining the temperature structure of the Irish Sea. *Journal of Physical Oceanography*, 33(11): 2288-2306.
- Holt, J.T., Proctor, R., Allen, J.I., Blackford, J., Ashworth, M.I. 2004. Advective controls on primary production in the stratified western Irish Sea: An eddy resolving model study. In press, *Journal of Geophysical Research*.
- James, I. D. 1986: A front-resolving sigma coordinate sea model with a simple hybrid advection scheme. *Applied Mathematical Modelling* 10: 87-92.
- James, I. D. 1996: Advection schemes for shelf sea models. *Journal of Marine Systems* 8: 237-254.

James, I. D. 2000: A high-performance explicit vertical advection scheme for ocean models: how PPM can beat the CFL condition. *Applied Mathematical Modelling*, 24(1), 1–9.

Mellor G. L. and Yamada T. 1974: A hierarchy of turbulence closure models for planetary boundary layers. *Journal of Atmospheric Sciences* 31:1791-1806.

Oey, L.-Y., 1998: Subtidal energetics in the Faroe-Shetland Channel: Coarse grid model experiments. *Journal of Geophysical Research* 103 C6:12689-12708.

Proctor, R., James, I. D. 1996: A fine-resolution three-dimensional model of the southern North Sea. *Journal of Marine Systems* 8: 285-295.

Proctor R., Holt J.T. and Balson P.S. 2001: Sediment Deposition In Offshore Deepes of the North Sea: Questions For Models. *Est. Coastal and Shelf Sci.*, 43 (4): 553-567.

Song, Y. & Haidvogel, D. 1994. A semi-implicit ocean circulation model using a generalised topography-following coordinate system. *J. Comp. Phys.*, 115: 228-244.

B2. Table of Moon States

Year	New Moon		First Quarter		Full Moon		Third Quarter					
2004	JAN	21	21:08	JAN	29	06:03	JAN	7	15:43	JAN	15	04:45
	FEB	20	09:21	FEB	28	03:27	FEB	6	08:50	FEB	13	13:39
	MAR	20	22:45	MAR	28	23:53	MAR	6	23:17	MAR	13	21:00
	APR	19	13:24	APR	27	17:39	APR	5	11:05	APR	12	03:47
	MAY	19	04:55	MAY	27	08:02	MAY	4	20:36	MAY	11	11:07
	JUN	17	20:29	JUN	25	19:11	JUN	3	04:21	JUN	9	20:07
	JUL	17	11:25	JUL	25	03:38	JUL	2	11:10	JUL	9	07:39
	AUG	16	01:24	AUG	23	10:10	JUL	31	18:06	AUG	7	22:06
	SEP	14	14:29	AUG	23	10:10	AUG	30	02:23	SEP	6	15:13
	OCT	14	02:48	SEP	21	15:51	SEP	28	13:09	SEP	6	10:12
	NOV	12	14:27	OCT	20	21:56	OCT	28	03:08	OCT	6	10:12
	DEC	12	01:29	NOV	19	05:49	NOV	26	20:08	NOV	5	05:53
2005	JAN	10	12:04	NOV	19	05:49	NOV	26	20:08	DEC	5	00:51
	FEB	8	22:30	DEC	18	16:40	DEC	26	15:07			
	MAR	10	09:13	JAN	17	07:00	JAN	25	10:33	JAN	3	17:43
	APR	8	20:35	FEB	16	00:20	FEB	24	04:55	FEB	2	07:25
	MAY	8	08:49	MAR	17	19:23	MAR	25	21:01	MAR	3	17:37
	JUN	6	21:58	APR	16	14:41	APR	24	10:09	APR	2	00:54
	JUL	6	12:05	MAY	16	08:59	MAY	23	20:21	MAY	1	06:30
	AUG	5	03:06	JUN	15	01:23	JUN	22	04:16	MAY	30	11:54
	SEP	3	18:46	JUL	14	15:19	JUL	21	11:03	JUN	28	18:29
	OCT	3	10:28	AUG	13	02:37	AUG	19	17:55	JUL	28	03:22
	NOV	2	01:24	SEP	11	11:35	SEP	18	02:02	AUG	26	15:18
	DEC	1	15:00	OCT	10	19:01	OCT	17	12:14	SEP	25	06:38
2006	DEC	31	03:12	NOV	9	01:58	NOV	16	00:57	OCT	25	01:13
	JAN	29	14:16	DEC	8	09:39	DEC	15	16:16	NOV	23	22:09
	FEB	28	00:33	JAN	6	19:60	JAN	14	09:48	DEC	23	19:35
	MAR	29	10:18	FEB	5	06:32	FEB	13	04:45	JAN	22	15:16
	APR	27	19:46	MAR	6	20:18	MAR	14	23:36	FEB	21	07:22
	MAY	27	05:28	APR	5	12:02	APR	13	16:42	MAR	22	19:17
	JUN	25	16:07	MAY	5	05:13	MAY	13	06:54	APR	21	03:34
	JUL	25	04:32	JUN	3	23:05	JUN	11	18:05	MAY	20	09:25
	AUG	23	19:11	JUL	3	16:36	JUL	11	03:04	JUN	18	14:10
	SEP	22	11:46	AUG	2	08:46	AUG	9	10:56	JUL	17	19:12
	OCT	22	05:15	SEP	30	11:05	SEP	7	18:44	AUG	16	01:48
	NOV	20	22:18	OCT	29	21:27	OCT	7	03:14	SEP	14	11:12
DEC	20	14:01	NOV	28	06:30	NOV	5	12:59	OCT	14	00:23	
2007	JAN	19	04:01	DEC	27	14:49	DEC	5	00:25	NOV	12	17:46
	FEB	17	16:15	JAN	25	23:03	JAN	3	13:58	DEC	12	14:35
	MAR	19	02:44	FEB	24	07:57	FEB	2	05:46	JAN	11	12:50
	APR	17	11:38	MAR	25	18:18	MAR	3	23:18	FEB	10	09:59
	MAY	16	19:29	APR	24	06:37	APR	2	17:16	MAR	12	04:01
	JUN	15	03:15	MAY	23	21:03	MAY	2	10:11	APR	10	18:08
	JUL	14	12:05	JUN	22	13:15	JUN	1	01:05	MAY	10	04:27
	AUG	12	23:04	JUN	22	06:29	JUN	30	13:50	JUN	8	11:40
	SEP	11	12:45	JUL	22	06:29	JUL	30	00:50	JUL	7	16:49
	OCT	11	05:02	AUG	20	23:54	AUG	28	10:37	AUG	5	21:16
	NOV	9	23:04	SEP	19	16:48	SEP	26	19:47	SEP	4	02:32
	DEC	9	17:41	OCT	19	08:33	OCT	26	04:53	OCT	3	10:08
			NOV	17	22:33	NOV	24	14:31	NOV	1	21:23	
			DEC	17	10:18	DEC	24	01:17	DEC	1	12:5	
									DEC	31	07:57	

Moon Phase data obtained from the Griffith Observatory Web Site. (www.griffithobs.org)
The Griffith Observatory is based on Los Angeles, USA.

B3. Additional Tidal Resource Details

CS3 Model: Peak Flow at Surface and Bed

Two quantities are provided:

- Mean Spring Peak Current (MSPC) - speed (m/s) followed by direction (degrees clockwise from North). Derived directly from ellipse parameters. This value is for depth-averaged currents, but the current at specified depths (1m below surface, 1m above sea bed) can be obtained by multiplying the depth mean current by the scaling factors provided; and
- Mean Neap Peak Current (MNPC) - speed (m/s) followed by direction (degrees clockwise from North). Derived directly from ellipse parameters. This value is for depth-averaged currents, but, as for MSPC, specific depth values can be obtained by multiplying by the scaling factors provided.

Scaling factors derived from Dept of Energy Guidance Notes (Dept of Energy, 1990) relate the current at any depth to the depth mean current through a simple two-part formula, found to give a good fit to profiles measured in a wide variety of locations:

$$u_t(z) = \left(\frac{z}{0.32H} \right)^{1/7} \bar{u}_t \quad \text{for} \quad 0 \leq z \leq 0.5H \quad (1)$$

$$u_t(z) = 1.065\bar{u}_t \quad \text{for} \quad 0.5 \leq z \leq H \quad (2)$$

where:

- \bar{u}_t = depth-averaged current at time t ;
- 0 = sea bed; and
- H = water depth (upwards).

This profile is typically accurate to $\pm 15\%$ throughout the water column, except very near the sea bed where local boundary layer effects and the type of bed form can influence very near bed currents.

From these expressions it is a simple matter to obtain current speeds at 1m below the sea surface ($z = H-1$) and 1m above the sea bed ($z = 1$).

CS3 Model: Conversion of Depth-Averaged Currents

The CS3 model calculates numerous current parameters which relate to a depth-averaged value. To obtain the current speed and power for different depths, an approximate scaling factor can be used (Table B3.1). These are also illustrated in Figure B3.1.

Table B3.1 Scaling factor used for calculating current speed and power at different depths

Depth (normalised)	Current Speed Scaling Factor	Power Scaling Factor
0.5 - 1 (mid-depth to surface)	1.066	1.211
0.4 - 0.5	1.051	1.162
0.3 - 0.4	1.014	1.045
0.2 - 0.3	0.967	0.906
0.1 - 0.2	0.900	0.730
0 - 0.1	0.760	0.450

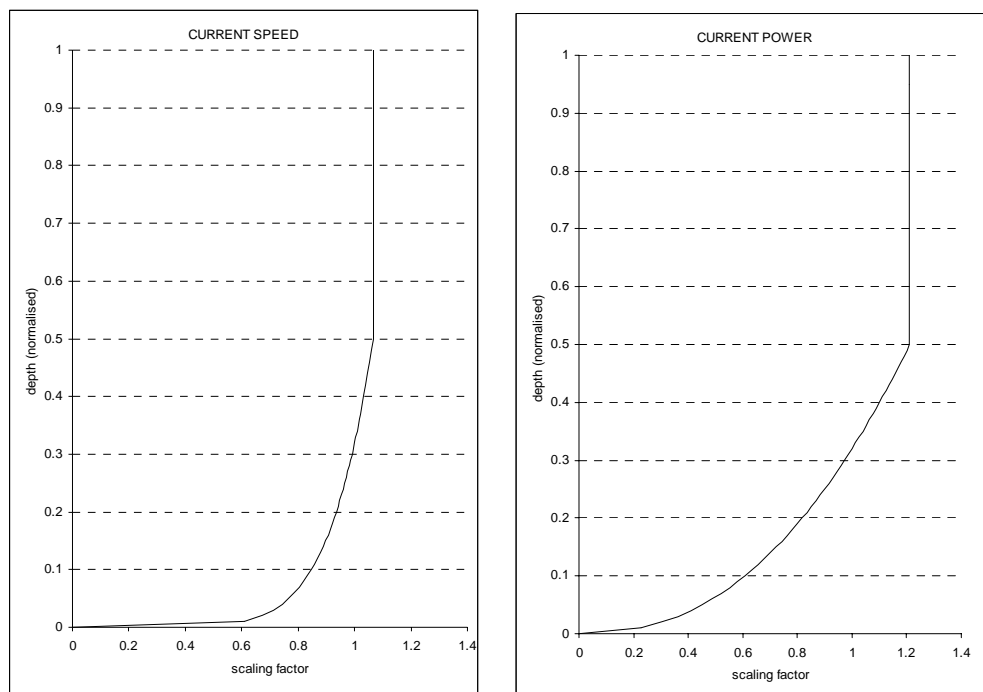


Figure B3.1 Scaling factor used for calculating current speed and power at different depths

HRCS Model: Conversion of Surface Currents

The HRCS model calculates numerous current parameters which relate to specific layers within the water column. Those presented in the Atlas relate to the surface and bed currents. To obtain the depth-averaged current speed and power, the surface current should first be divided by 1.065832 and then the scaling factors defined in Table B3.1 applied.

Persistence Values

These are provided via a Frequency Distribution giving the percentage time the current (either at 1m below the surface or 1m above the sea bed) is within a specified range of speeds. The upper limits (in m/s) for each of the intervals are:

0.2, 0.4, 0.6, 0.8, 1.0, 1.2, 1.4, 1.6, 1.8, 2.0, 2.2, 2.4, 2.6, 2.8, 3.0, 3.5, 4.0, 4.5, 5.0,

The distribution is determined from hourly current values over a one year period (here 2001 was selected). It was found that a higher frequency of sampling had an insignificant impact on the results.

Spring-Neap Variability

Tides in the UK coastal waters exhibit a Spring-Neap amplitude variation over successive 15 day periods. The fractional increase, α , relative to the mean (M_2) tide is typically 0.35 with a maximum of 0.5 (varying systematically with location and over the annual cycle).

Since tidal power is proportional to tidal current U to the third power, maximum power generation varies by the following ratios:

for $\alpha = 0.5$, 3.375 (greater) on Springs and 0.125 (smaller) on Neaps and on average (over the Spring- Neap cycle) by:

$1+1.5 \alpha^2$, i.e. by 1.375 for $\alpha = 0.5$.

Total Potential and Sensitivity to Extraction

Flather (1976) estimated net tidal energy dissipation rates for the mean (M_2) tide as follows:

NW Shelf Seas 200GW

Irish Sea 30GW

This Shelf Sea tidal energy is generated in the Atlantic Ocean, its subsequent propagation pathways can be calculated, for each tidal constituent, from

$$0.5 \rho g D Z U \cos(\theta) \quad (3)$$

where

θ is the phase lag of tidal elevation Z relative to tidal velocity U , D = depth)

Thus the net energy transmitted across any chosen section can be calculated. For an enclosed region, the net energy dissipated by bed friction will equal the sum transmitted across the boundaries.

The energy values increase by up to a factor of 3.5 on spring tides and by, typically, 1.35 averaged over the Spring-Neap cycle- via the contributions from other tidal constituents.

For a turbine diameter ϵD (D = water depth) the maximum Kinetic Energy extraction per unit breadth is $0.125 \rho \pi \epsilon D U^3$.

(ρ = density, D = water depth, U = tidal velocity)

Energy is dissipated by friction at the sea bed at a rate $\rho C U^3$, where the bed stress coefficient $C \sim 0.0025$. Hence the energy extracted is equivalent to that dissipated over a distance

$$L = 50 \pi \epsilon D \quad (4)$$

i.e. about 4 km for $\epsilon=0.5$ and $D=50\text{m}$.

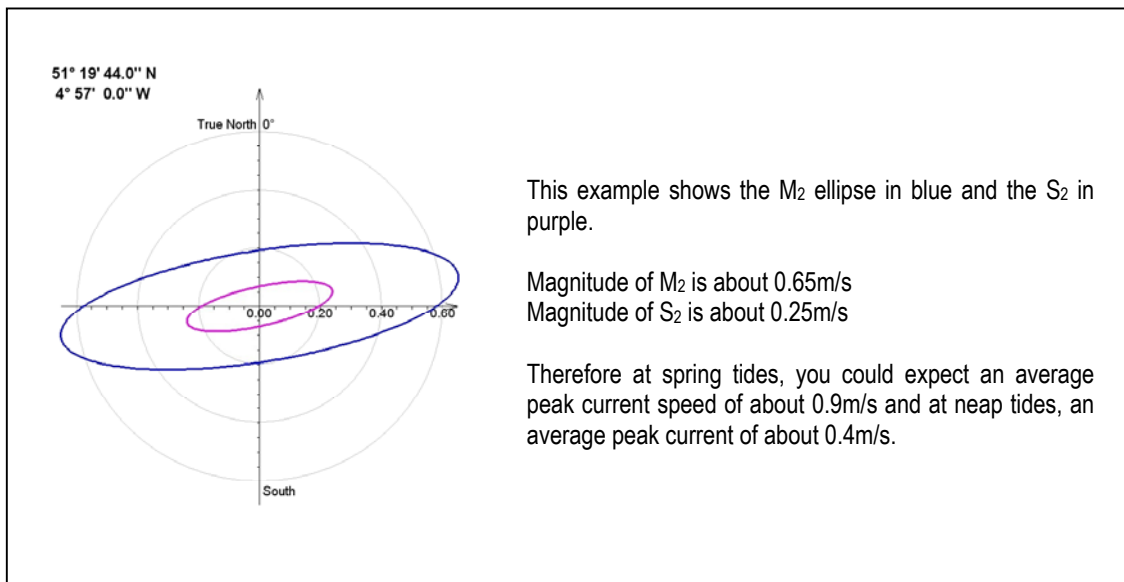
Tidal Current Ellipses

The two principle components of the tide are known as the M_2 and S_2 . The M_2 component is the twice-a-day (semi-diurnal) tide that is caused by the moon and has a period 12 hours 25 minutes 14.16 seconds. The S_2 component is the semi-diurnal tide caused by the sun and has a period of exactly 12 hours.

Due to the different time periods of the M_2 and S_2 , these two components move in and out of phase over a 29.5306 day cycle. Spring tides occur when the M_2 and S_2 are either completely in phase or completely out of phase (hence the spring-neap cycle being exactly half the lunar phase cycle).

During spring tides, the M_2 and S_2 components reinforce each other. Therefore an indication of the average magnitude of spring tidal currents can be obtained by summing the magnitude of M_2 and S_2 shown on the tidal ellipse output together.

To get an estimate of the magnitude of neap tidal currents, the S_2 component should be subtracted from the M_2 component.



The major axis of the M_2 ellipse shows the principle direction of current flow. The S_2 ellipse major axis is nearly always oriented within $\pm 15^\circ$ of the M_2 ellipse. In the example above, the current flow is primarily on a bearing of 080° and 260° .

The 'fatness' of the ellipse gives an indication of how much time the current is flowing in a direction close to the principle axis. A very thin ellipse will be flowing for most of the tidal cycle very close to the major axis with the current reversing direction very quickly. This is a desirable flow pattern for current turbine technology. A more circular ellipse indicates a current which changes direction more gradually, spending less time flowing in a direction close to the major axis.

References

Department of Energy. 1990. Metocean parameters – parameters other than waves. Supporting document to Offshore Installations: Guidance on Design, Construction and Certification – Environmental considerations. Offshore Technology Report. 151 pp. (see page 55).

Flather, R.A. 1976. A tidal model of the NW European Continental Shelf. *Memoires Societe Royale des Sciences de Liege*. 6(10):141-164.

B4. Validation of the POL Numerical Scheme

HRCS Model Scheme

Tidal Elevations

Six tidal components, representing the more important tidal components, have been selected for assessment here, these are the diurnal constituents O_1 and K_1 , semi-diurnal constituents N_2 , M_2 , S_2 and quarter-diurnal constituent M_4 . These are compared against data contained within the BODC which consists of 257 coastal and offshore tide gauges and 278 current meter instruments.

Figure B4.1 shows the comparison between the amplitudes of the BODC and model datasets for these six components. The scatter plots show model and observed values together with a line of perfect agreement and show that the model is generally in good agreement with the observed tidal constituents. This is further supported by the mean and root mean square (RMS) differences (shown above each plot and provided in Table B4.1). The greatest discrepancy is in the Bristol Channel where the observed high tidal range is overestimated by the model, most noticeably in the M_2 . More scatter is noticeable in the higher harmonic M_4 indicating, probably, the highly local nature of the generation mechanism of this constituent.

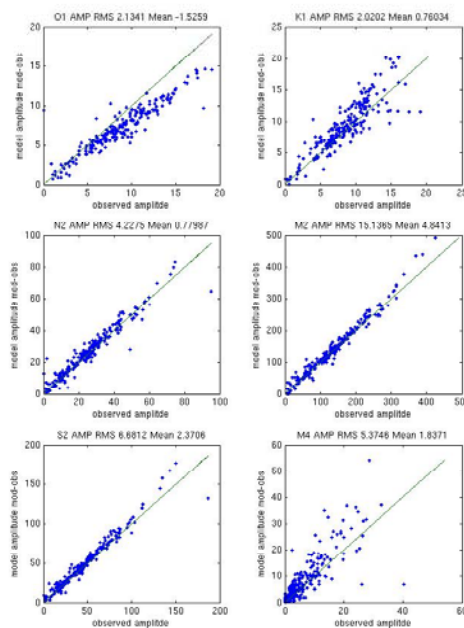


Figure B4.1 Scatter plots of model vs. observed tidal amplitudes

Table B4.1 Error statistics for the tidal elevations

Constituent	Amplitude (cm)		Phase (degrees)	
	RMS	Mean	RMS	Mean
O ₁	2.1	-1.5	19.3	-3.2
K ₁	2.0	0.8	30.6	-9.3
N ₂	4.2	0.8	27.7	-3.7
M ₂	15.1	4.8	25.1	5.7
S ₂	6.7	2.4	22.9	-3.0
M ₄	5.4	1.8	71.8	22.2

Figure B4.2 shows similar scatter plots for the phase of the tidal constituents and the error statistics are also given in Table B4.1. These indicate small phase errors.

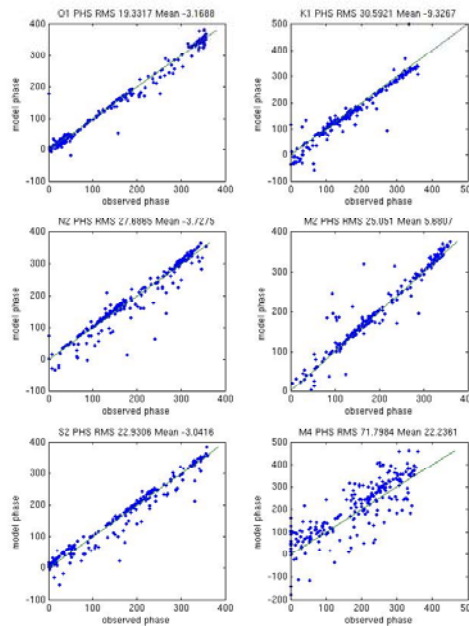


Figure B4.2 Scatter plots of model vs. observed tidal phases

To indicate the spatial error variability, Figure B4.3 shows the error between the model and observed in M₂ amplitude and phase for all the available data points. This figure clearly indicates the overall good agreement between observed and computed tidal elevations over the UKCS.

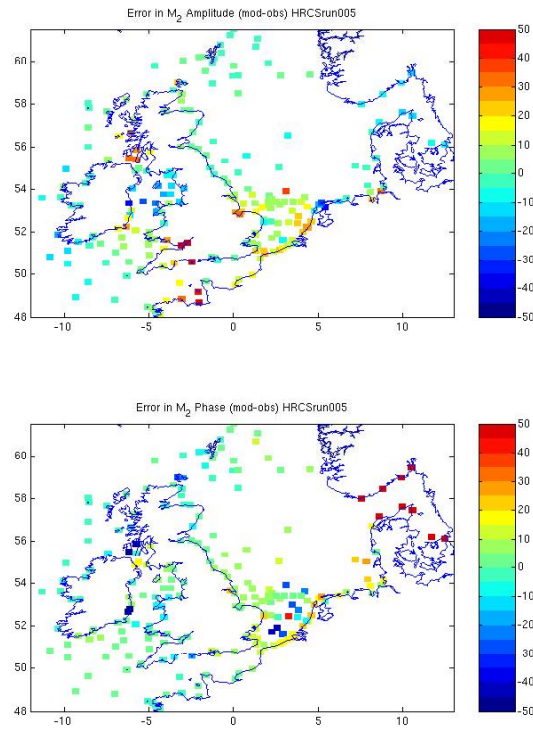


Figure B4.3 Spatial distribution in differences (model – observed) for M_2 amplitude (cm, upper) and phase (degrees, lower)

Tidal Currents

For the tidal currents, all 278 available BODC current meter data was extracted and compared with modelled currents. A subset of these comparisons is provided here.

Figure B4.4 shows the model and observed differences in speed and direction for the semi-major component of the M_2 tidal ellipse. This was calculated for the uppermost (i.e. the highest above the sea bed) current meters. Where a current meter mooring consisted of one instrument this was used whilst if there was more than one instrument on a mooring, the upper most was used. Therefore it is the errors in the strongest tidal currents that are shown, as in general tidal currents become weaker closer to the sea bed. It is shown that the model has, in general, small errors in both speed and direction, when compared to the BODC observations.

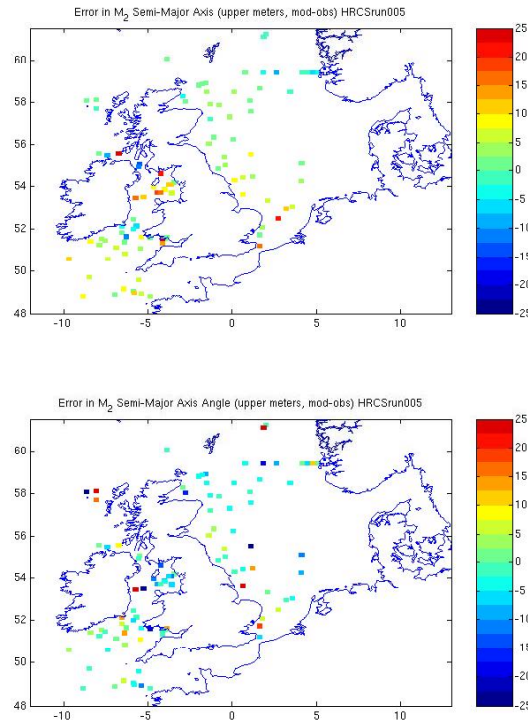


Figure B4.4 Spatial distribution in differences (model – observed) for speed (cm/s, upper) and direction (degrees, lower) of M_2 semi-major axis of tidal ellipse

A statistical analysis has also been carried out. Table B4.2 shows the mean and RMS differences between the model and observed semi-major axis of the tidal ellipse for the same six constituents presented in the tidal elevation comparison.

Table B4.2 Error statistics for tidal current speed (cm/s)

Constituent	RMS	Mean
O_1	0.71	-0.36
K_1	1.07	0.09
N_2	2.00	0.25
M_2	6.85	2.18
S_2	2.83	1.02
M_4	1.25	0.13

Figure B4.5 shows the model vs. observed scatter plots for this parameter. This plot differs slightly in construction to the scatter plots of tidal elevation.

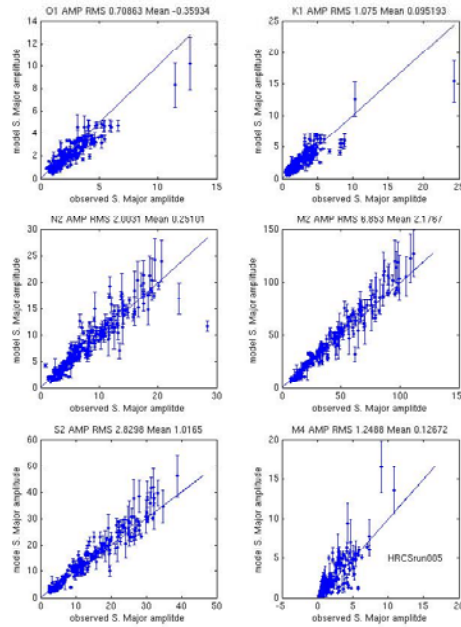


Figure B4.5 Plots of model vs. observed semi-major axis tidal current speeds (cm/s)

Here, to give some indication of the tidal current variability (which are expected to be greater than for the tidal elevations due to the larger influence of topography/bathymetry on the current structure) a mean model semi-major axis current speed and a model standard deviation for a 12 km x 12km area surrounding the current meter location has been calculated, for each observation point (k):

$$mean\ s-m\ axis_k = \frac{1}{M} \sum_{i=-3}^3 \sum_{j=-3}^3 s - m\ axis_{k-(i,j)} \quad (1)$$

where

- i = east-west element;
- j = south-north element.

In open water, $M = 7 \times 7 = 49$. Elements within the search area that are on land are omitted and M is reduced accordingly.

$$standard\ deviation = \sqrt{\frac{1}{M-1} \sum_{i=-3}^3 \sum_{j=-3}^3 (s - m\ axis_{k-(i,j)} - mean\ s - m\ axis_k)^2} \quad (2)$$

Therefore for each point in the scatter plot there is a model mean value and a standard deviation error bar which indicates the range of the modelled current within the 12km square box. It is clear that for most tidal components the model is, in general, in good agreement with the observations. The spread, which in general increases with current speed, shows the variability due to bathymetry which might be expected within a 12km square box, indicating the care which should be exercised when comparing observed data with model data.

HRCS vs. CS3

Comparison between the HRCS and CS3 model output does show that, whilst the overall description of the tidal resource is similar, there are subtle differences which result from :

1. the different spatial horizontal resolution of the two schemes. CS3 uses, approximately, 12km grid cells whilst the HRCS uses 1.8km cells; and
2. the different vertical resolution of the two schemes (CS3 is depth-averaged whilst the HRCS is defined with 34 layers throughout the water column).

Thus, when comparing the surface current speeds from the HRCS model (Figure B4.6) with the current speeds from the CS3 model (Figure B4.7), the higher values are typically of a greater magnitude and cover a wider area in the former as the smaller values experienced in the lower water column are not taken into account. In order to provide details on the lower current speeds, and thus the variation through extremes, one should examine the near-bed current speeds provided by the HRCS model. The CS3 model therefore provides a current speed which 'sits' between these two extremes. A similar explanation exists for the comparison of all tidal parameters from these two models.

HRCS vs. Seapower South West

The Seapower South West study used the UK Shelf Model to derive tidal parameters. This model was developed by Pingree at Plymouth Marine Laboratories and further details on the these model can be found in Metoc (2004). Comparisons between the two studies have been made both using the tidal and wave resources. As with the comparison between the HRCS and CS3 models, similarities do exist between these and the Seapower model (Metoc, 2004). However, as with the former two, differences do exist which result from the Seapower model having a horizontal resolution of 5km and being depth-averaged in the vertical. Thus, the HRCS provides a higher resolution of data.

Reference

Metoc (2004). Seapower SW Review : Resources, constraints and development scenarios for wave and tidal stream power in the south west of England. Metoc Report Number 1220.